

3ZnO/TiO₂ Coupled Oxides LLDPE Nanocomposite: Effect of Various Weight Percent of Sol-gel Synthesized Catalyst on Structural and Bacteriostatic Activity Against *S. Aureus* and *E. Coli*



Khairul Arifah Saharudin¹, Srimala Sreekantan*¹, Norfatehah Basiron¹, Rabiatul Basria SMN Mydin², Nor Hazliana Harun², Lim Jit Kang³ and Azman Seeni⁴

¹School of Materials & Mineral Resources Engineering, Universiti Sains Malaysia, Malaysia

²Advanced Medical and Dental Institute, Universiti Sains Malaysia, Malaysia

³School of Chemical Engineering, Universiti Sains Malaysia, Malaysia

⁴Malaysian Institute of Pharmaceuticals and Nutraceuticals (IPHARM), National Institute of Biotechnology Malaysia, Ministry of Science, Malaysia

Received:  August 19, 2018; Published:  September 04, 2018

*Corresponding author: Srimala Sreekantan, School of Materials & Mineral Resources Engineering, Engineering Campus, Universiti Sains Malaysia, 14300 Nibong Tebal, Pulau Pinang, Malaysia

Abstract

In this study, coupled oxide 3ZnO:1TiO₂ (3ZT) synthesized by sol-gel method with different weight percentage were incorporated in linear low-density polyethylene (LLDPE) for antimicrobial application. The nanoparticles were homogeneously distributed across the surface due to the casting method adopted in this work. The formation of heterojunction of 3ZT and crystalline nature of the phases and high quantity of surface 'OH resulted in LLDPE nanocomposites with higher adsorption water molecules property, thus causing a substantial improvement in photocatalytic reaction. The antimicrobial results indicate LLDPE incorporated with coupled oxide 3ZT was active in inactivating Gram-positive; *Staphylococcus aureus* (*S. aureus*) and Gram-negative; *Escherichia coli* (*E. coli*). *S. aureus* was found to be more susceptible in killing as compared to *E. coli*, under visible light. The best inactivation up to 100% was able to achieve for both bacteria in LLDPE with 10wt.% under visible light due to more Zn ion and 'OH release at a specific incubation time.

Abbreviations: LLDPE: Linear Low-Density Polyethylene; ZAD: Zinc Acetate Dehydrate; Ag: Silver; Cu: Copper; TiO₂: Titanium Dioxide; ZnO: Zinc Oxide; GRAS: Generally Recognized As Safe; TTIP: Titanium Isopropoxide; DSC: Differential Scanning Calorimetry; Tm: Melting Temperature; FTIR: Fourier Transform Infrared Spectrometer; HRTEM: High-resolution Transmission Electron Microscopy; MB: Methylene Blue; BQ: Benzoquinone; AMDI: Advanced Medical and Dental Institute; LB: Luria-Bertani; CFU: Colony Forming Unit; DSC: Differential Scanning Calorimetry; ACN: Acetonitrile; NCLS: National Committee for Clinical Laboratory Standards; MOE: Ministry of Education; TRGS: Transdisciplinary Research Grant Scheme; USM: Universiti Sains Malaysia

Introduction

Microbial contamination poses a major threat to human health. Many diseases spread due to the bacterial infections, which cause significant economic and personal losses [1]. Hence, antimicrobial modification of surfaces to prevent growth of detrimental microorganism is highly desired. In biomedical devices such as catheters, prosthetics and implants, surface microbial invasion can result in serious infection and device failure [2]. Surface-centered infections also implicated in food spoilage, spread of foodborne disease and biofouling of materials [3]. Hence, there is significant interest in the development of antimicrobial materials and surfaces for applications in the health and biomedical device industry, food industry and personal hygiene industry. Incorporation of antimicrobial agents directly into polymers [4-6] have gained

priority in research [7] due to unique properties such as strong antibacterial activity at low concentrations [8], stable in extreme conditions [9], non-toxic [10], and some of them even contain mineral elements essential to the human body [9]. Various metal and metal oxides such as silver (Ag), gold (Au), copper (Cu), titanium dioxide (TiO₂), and zinc oxide (ZnO) has been incorporated in polymeric materials [11,12].

Among them TiO₂ has been one of the most versatile antimicrobial agents due to its excellent photocatalytic antimicrobial activity over a broad spectrum of microorganism. The antimicrobial properties of TiO₂ are attributed to the high redox potential of ROS generated by the photo-excitation. Chawengkijwanich and Hayata, [13] developed TiO₂ powder-coated packaging film and

verified its ability to reduce *E. coli* contamination on food surface. TiO₂ nanoparticles was reported to kill viruses including hepatitis B virus [14] and herpes simplex virus [15]. Recently, Ramesh and co-workers [16] reported the potential application of TiO₂ photocatalyst in the food sector. The U.S. FDA has approved the use of TiO₂ in human food, drugs, cosmetics and food contact materials [17]. Zinc oxide (ZnO) is frequently considered as an alternative to TiO₂ for photocatalytic applications [18]. Currently, it is listed as one of five zinc compounds that is generally recognized as safe (GRAS) by the U.S. FDA [17]. Wang et al. [19] reported ZnO nanoparticles exhibit strong antibacterial property over a broad range of microorganism. Azam and co-workers [20] found that ZnO has the highest bactericidal activity against both Gram-negative (*E. coli* and *P. aeruginosa*) and Gram-positive (*S. aureus* and *B. subtilis*) bacteria compared to CuO and Fe₂O₃ nanoparticles. Nevertheless, the potential of single phase TiO₂ and ZnO to achieve complete inactivation is hindered due to high recombination of electron and holes. Besides, the incorporation of these particles in polymer matrix further reduce the water uptake, ion and ROS migration thus reduce their inactivation capacity.

Attempt has been made to combined TiO₂ and ZnO particles to improve its individual antimicrobial property. These particles would gallop the properties of both of the nanoparticles simultaneously while retaining their individual characteristics. There have been multiple reports of these coupled oxides which perform dually well when combined than in their individual states [21-23]. However, most of the literatures concerning only on coupled oxides nanoparticles and not polymer nanocomposites. In our previous work, bacteriostatic activity of LLDPE nanocomposite embedded with sol-gel synthesized TiO₂/ZnO coupled oxides with various ratios at 5wt.% has been reported [24]. However, the effect of various percentage of best performed catalyst 3ZT was not addressed in the reported work. Besides total inactivation of *S. aureus* was not achieved. Therefore, in this work structural aspects, metal ion and ROS release of LLDPE nanocomposites with various percentage (1, 3, 7, 10 wt.%) 3ZT and prolonged incubation time for complete inactivation of Gram-positive; Staphylococcus aureus (*S. aureus*) and Gram-negative; Escherichia coli (*E. coli*) is performed. The structural and functional relationship and the resultant outcomes of this work have the potential benefits to design antimicrobial polymer nanocomposites that function under visible light to reduce disease transfer via biomedical devices.

Experimental

Materials

The chemicals used in this study were Titanium (IV) isopropoxide (97%, supplied by Sigma Aldrich), Zinc acetate dehydrate (98%, supplied by Sigma Aldrich), Deionized water, Methylene Blue (Merck), Ethanol (95%, supplied by Biotech Lab Supplies) and 1,2-dichlorobenzene (Merck). LLDPE pellets were obtained from Lotte Chemical Titan (M) Sdn. Bhd. (Kuala Lumpur,

Malaysia). All the chemicals and materials mentioned were used as purchased without further purification.

Preparation of 3ZT Coupled Oxide

In this study, sol-gel process was carried out to synthesis the 3ZT coupled oxide of 1:3 molar ratio of TiO₂ and ZnO. The ZnO nanoparticles were prepared as follows. ZnO sol was prepared by adding 0.114 mole Zinc acetate dehydrate (ZAD) into ethanol. The solution was stirred for 5 min in heated (70 °C) water bath to obtain the precursor solution. Next, continuous stirring for 5 h were carried out until transparent solution is obtained. Then, deionized water was added drop wise and stirred for 10 min. On the other hand, the TiO₂ nanoparticles were prepared by dissolving Titanium Isopropoxide (TTIP) in ethanol with the volume ratio of 1:4 and stirred for 30 min. Then, deionised water was added dropwise and stirred for 3 h. After TiO₂ and ZnO sols are synthesized separately, the sols are mixed to different (TiO₂: ZnO) molar ratio and stirred continuously for 1h. The milky white suspension was centrifuged, washed with ethanol until white sediment was observed. The resultant sediment was oven dried overnight at 80 °C. The dried white precipitate was pulverized with pestle and mortar and calcined in air at 500 °C for 2h.

Preparation of LLDPE Nanocomposite

The LLDPE nanocomposites denoted as LLDPE/3ZT/1, LLDPE/3ZT/5, LLDPE/3ZT/7 and LLDPE/3ZT/10 were prepared from the mixture containing 1 g of LLDPE matrix and 1, 5, 7 and 10 wt% of 3ZT coupled oxide. Each mixture was prepared separately. 1 g LLDPE pellets were dissolved into 15 ml of 1,2-dichlorobenzene at 70 °C under continuous stirring for 10 min. While 1 wt.% of coupled oxide were added into 10 ml of 1,2-dichlorobenzene and sonicated for 3 min. After the LLDPE pellets were completely dissolved by 1,2-dichlorobenzene, the coupled oxide solution was added drop wisely into the polymer melt and stirred for 1 min. Finally, the mixture solution was poured into 90 mm diameter petri dish and oven dried at 80 °C for 18 h. Then, the mixture was allowed to continuous stir for 1 min to allow homogeneous mixing. The solution mixture was then poured into a 90 mm diameter petri dish and allowed to oven dry for 18 h [25,26]. The procedure was repeated for the rest of wt.% of 3ZT coupled oxide.

Characterization

The melting temperature (T_m) and the enthalpy of fusion (ΔH_f) were determined using differential scanning calorimetry (DSC, Mettler Toledo). Each nano-composite with ~15 – 20 mg was weighed and scanned from room temperature to 200 °C at a heating rate of 20 °C/min in an inert nitrogen (N₂) atmosphere (N₂ flow rate of 50 ml/min). The relative crystallinity was calculated from the enthalpy value (ΔH); the parameter value for 100% crystalline LLDPE was 276 J/g [27]. The relative crystallinity was calculated based on the following equation [28].

$$(1-\lambda)\% = \frac{\Delta H_f}{\Delta H_{f100\%} \cdot w} \times 100$$

w = weight fraction of the filler or matrix in blends, ΔH_f = apparent enthalpy of melting of the filler or matrix, $\Delta H_{f100\%}^0$ = extrapolated value of the enthalpy that corresponded to the melting of 100% crystalline sample (276 J/g for LLDPE). The chemical structure of bare and LLDPE nanocomposites were confirmed using a Fourier transform infrared spectrometer (FTIR, Tensor27, Bruker, Germany). The high-resolution transmission electron microscopy (HRTEM) images and selected area electron diffraction patterns were obtained using a TECNAI G2 20 S-Twin instrument. The crystalline phases were analyzed using X-ray diffraction (XRD, X-Ray diffractometer D8 Advance BRUKER AXS GMBH). The metal ions released from the LLDPE nanocomposites were quantified using an inductively coupled plasma-optical emission spectrometer (ICP-OES Optima DV Perkin Elmer Inc., Branford, CT, USA). Each LLDPE nanocomposite film was (60 mm in diameter) immersed into a solution of 100 mL of deionized water, wherein 3 mL from the solution had been analyzed at 12, 24, 48, 72, and 96 h.

The role of reactive species from LLDPE nanocomposites was determined by testing the photocatalytic activity of the nanocomposite films to degrade methylene blue (MB) aqueous solution. The film was immersed in 10 ppm of 40 mL of MB and kept in dark for 1 h to attain an equilibrium adsorption state. In order to determine the photodegradation efficiency under sunlight, a number of experiments were performed from 11:00 until 14:00. At fixed time interval, the LLDPE film was removed, while the solution was withdrawn and measured using a UV-vis spectrophotometer at 644 nm. The reactive species ($\cdot\text{OH}$, $\text{O}_2^{\cdot-}$, h^+) formation due to photoinduced process over LLDPE nanocomposites were monitored by 5 mmol/L methanol (MeOH), acetonitrile (ACN), and benzoquinone (BQ) as scavengers for h^+ , $\cdot\text{OH}$ radical, and superoxide anion radical $\text{O}_2^{\cdot-}$, respectively.

Bacterial Strains, Media and Materials

To evaluate the antibacterial properties of LLDPE nanocomposites with different weight percentage of 3ZT coupled oxide, two types of strain, known as Gram positive *Staphylococcus aureus* (ATCC 25923) and Gram-negative *Escherichia coli* (ATCC 25922) an obtained from Advanced Medical and Dental Institute (AMD) (Bertram). Both microorganisms were subculture aerobically at 37 °C in Luria-Bertani (LB) broth, (Merck, Germany) for 16-18 h.

Standard Test Method under Dynamic Conditions

The antibacterial effectiveness of LLDPE nanocomposites with different percentage of 3ZT coupled oxide was assessed against *S.*

aureus (ATCC 25923) and *E. coli* (ATCC 25922) using the standard test method ASTM E 2149-01 (ASTM Designation E 2149-01). Briefly, bacterial inoculum was prepared in sterile nutrient broth (Luria-Bertani) and left overnight at 37°C, 115rpm. Then, the bacterial inoculum was diluted using a sterile buffer solution (0.3mM KH_2PO_4) until the solution adjusted to 0.28 ± 0.02 for *E. coli* and *S. aureus* at 475 nm which corresponds to $1.5\text{-}3.0 \times 10^8$ (CFUs/mL). A LLDPE nanocomposite thin film with a $2.7 \times 2.7 \text{ cm}^2$ was placed in a conical flask comprising 50 mL sterile buffer solution and 0.1 mL of both inoculums (*S. aureus* and *E. coli*) was added after being maintained to a strain concentration of $1.5\text{-}3.0 \times 10^5$ CFUs/mL as the working bacterial dilution. The conical flasks were shaken (115 rpm) for 1, 6, 12, and 24 h at 37 °C using a mechanical shaker under visible light.

After incubation time of 1 h, 100 μl aliquots of appropriate dilution were placed in LB agar and incubated for 24 h at 37°C. Later, the colony forming unit (CFU) of each plate were determined. Colonies were counted and compared to those on control plates to measure changes in the cell growth inhibition. The bare LLDPE nanocomposite and bacterial inoculum only served as control. The percentage of bacteria reduction (R %) was calculated using the following equation: $R\% (\text{cfu} / \text{mL}) = [(B - A) / B] \times 100$, where R is antibacterial rate (%), B are the average number of cell colony of blank sample (CFU/sample) and A are the average number of colony of treated sample (CFU/sample) at specified contact time.

Results and Discussion

Differential scanning calorimetry (DSC) is one of the most important techniques of thermal analysis for studying the crystallization characteristics of polymeric materials and composites. DSC data for bare LLDPE and LLDPE nanocomposites with 1 - 10 wt.% 3ZT coupled oxide including melting point, crystallization temperature, heat of melting and percentage of crystallinity are summarized in Table 1. From Table 1, insignificant changes in the T_c and T_m of the LLDPE and its nanocomposites suggest the wet casting method does not alter the melting behavior of the LLDPE nanocomposites. However, it can be seen from (Table 1) that the crystallinity of the LLDPE decreased by 6.5% with maximum of 7 to 10 wt% addition of coupled oxide. This behavior indicates that 3ZT coupled oxides with high degree of crystallinity inhibits spherulitic growth and does not co-crystallize with LLDPE to form crystalline LLDPE structure. Therefore, the degree of crystallinity for LLDPE nanocomposites was relatively lower than bare LLDPE, hence contributing to more amorphous region for water uptake to initiate photocatalytic reaction of 3ZT for microbes' inactivation.

Table 1: The percent crystallinity, X_c of bare LLDPE and LLDPE nanocomposites with 1 to 10 wt% 3ZT coupled oxide.

Sample	T _c (°C)	T _m (°C)	Apparent enthalpy H' (J/g) = Enthalpy of fusion, H _m - Enthalpy of crystallisation, H _c	Enthalpy of melting of 100% crystalline LLDPE, ΔH ₀ (J/G)	Percent crystallinity, X _c (%)
LLDPE	36.5	106.7	52.53	276	19.03
LLDPE/3ZT/1	36.5	106.5	20.12	276	14.04
LLDPE/3ZT/3	36.5	106.7	17.03	276	14.37
LLDPE/3ZT/7	36.5	106.5	15.67	276	12.59
LLDPE/3ZT/10	36.5	106.5	13.58	276	12.46

The FTIR spectra of 3ZT coupled oxide, bare LLDPE and LLDPE nanocomposites with 1– 10 wt.% 3ZT coupled oxide are shown in Figure 1. The FTIR spectrum of 3ZT coupled oxide Figure shows a broad and intense peak at 3407.86 cm⁻¹ corresponded to the hydroxyl groups of chemisorbed water molecules on the samples [29]. The peak at 2328.66 cm⁻¹ results from the adsorbed H₂O molecules [30]. Besides, a physisorbed water molecule was present indicated by the peak at 1642.27 cm⁻¹. Meanwhile, Zn-O stretching of ZnO is visible at 609.69 cm⁻¹. For bare LLDPE, representative band of polyethylene were observed in the regions of 3500 – 2800 cm⁻¹, 1700 – 1000 cm⁻¹ and 750 – 650 cm⁻¹. The strong peak at 2907.04 cm⁻¹ and 2842.87 cm⁻¹ is attributable to the C-H stretching vibrations of CH₂ and CH groups [31]. Another band at 1656.76 cm⁻¹ was related to CH₃ bonding deformation. The weak band at 1376.62 cm⁻¹ was assigned to CH₃ symmetric deformation and a medium band at 722.5 cm⁻¹ was attributed to the rocking deformation. In the LLDPE nanocomposites, all the characteristics peak of bare LLDPE were retained except for a band at 1642.27 cm⁻¹ and 3403.15 cm⁻¹ associated with OH vibration of adsorbed water and OH bending vibration that originated from the 3ZT coupled oxide characteristic.

However, compare to 3ZT coupled oxide spectrum, the intensity of these bands possesses lower intensity due to the evaporation of adsorbed water during nanocomposites preparation. The preservation of LLDPE characteristics in LLDPE nanocomposites indicate that the chemical structures were preserved without forming appreciable chemical bonding between LLDPE and 3ZT coupled oxide (Figure 1).

In order to evaluate the ROS release from the LLDPE nanocomposites with different weight percentage, photodegradation of MB was performed and the results are shown in Figure 2. The photo-degradation of MB under visible light respond by LLDPE nanocomposite that contains 1, 3, 7 and 10 wt.% 3ZT are 90%, 96%, 100% and 100%, respectively. The results show pronounced improvement in the MB degradation with increasing 3ZT content, corresponding significant ROS release from LLDPE nanocomposites within 4 h. The degradation rate of MB aqueous solutions containing LLDPE nanocomposites with different weight percent is shown in Figure 3 and the results indicates the performance follow the pseudo-first-order kinetics with respect to the concentration of

dye in bulk solution (C):

$$-\frac{dc}{dt} = k_{app} C$$

Integration of that equation (with the same restriction of C = C₀ at t = 0, with C₀ being the initial concentration in the bulk solution after dark adsorption and t the reaction time) will lead to the expected relation: ln

$$\frac{C_0}{C} = k_{app} t$$

in which k_{app} is the apparent pseudo-first-order rate constant and is affected by MB concentration. The value of k_{app} can be obtained directly from the regression analysis of the linear curve in the plot. It can be clearly observed that LLDPE/3ZT/7 nanocomposite showed the highest photocatalytic activity with a corresponding k_{app} value of 1.8 x 10⁻⁴ h⁻¹, followed by LLDPE/3ZT/10, LLDPE/3ZT/3 and LLDPE/3ZT/1 with a k_{app} value of 1.4 x 10⁻⁴, 0.9 x 10⁻⁴ and 0.2 x 10⁻⁴ h⁻¹, respectively. The fast photodegradation rate of 7 and 10 wt.% of 3ZT in LLDPE polymer nanocomposites under visible light was one of the best results achieved compared to other reported work [32]. This is attributed to the heterojunction formation of ZnO/TiO₂ coupled oxides (Figure 4) that increase the recombination resistance and lifetime of photogenerated carriers, which is resulted from the charge separation. HRTEM image shown in Figure 4a verify the heterojunction formation within 3ZT coupled oxides. As seen, there are two lattice fringes with interplanar spacing of 0.58 nm (Figure 4b) and 0.56 nm (Figure 4c) associated with two different crystal structures. XRD diffraction pattern in Figure 4d reveals the lattice fringes with interplanar spacing of 0.52 nm corresponding to hexagonal ZnO crystals while 0.58 corresponding to the of cubic-Zn₂Ti₃O₈.

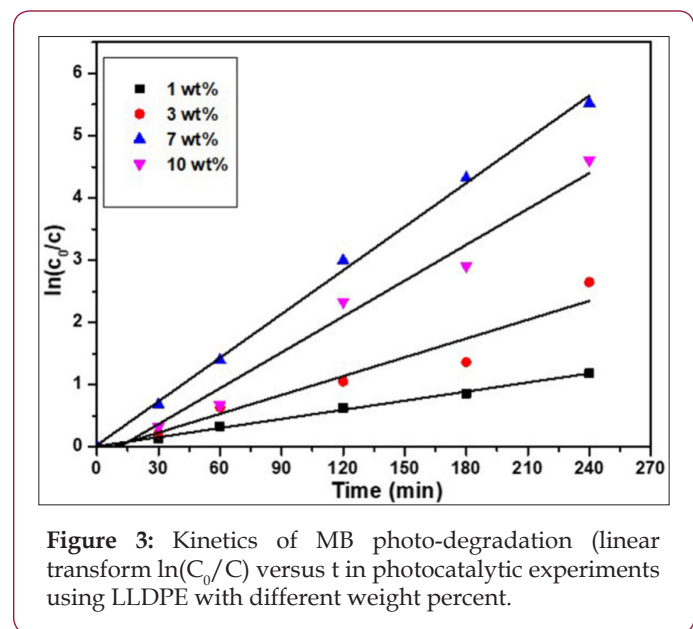
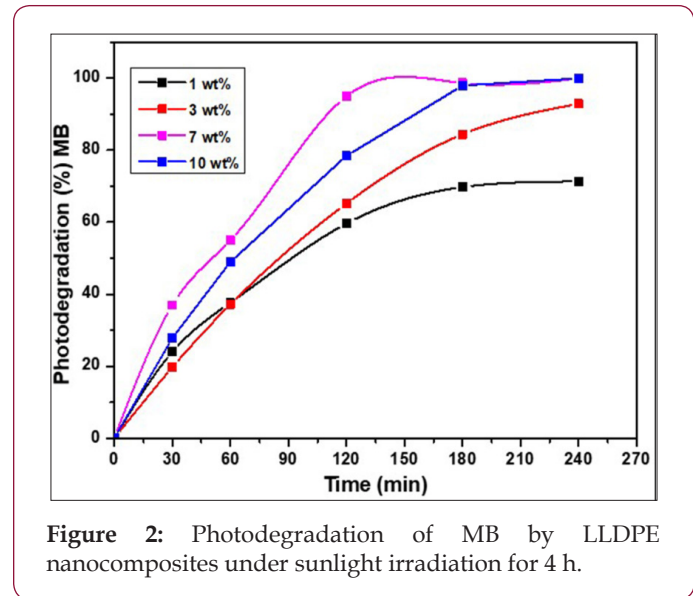
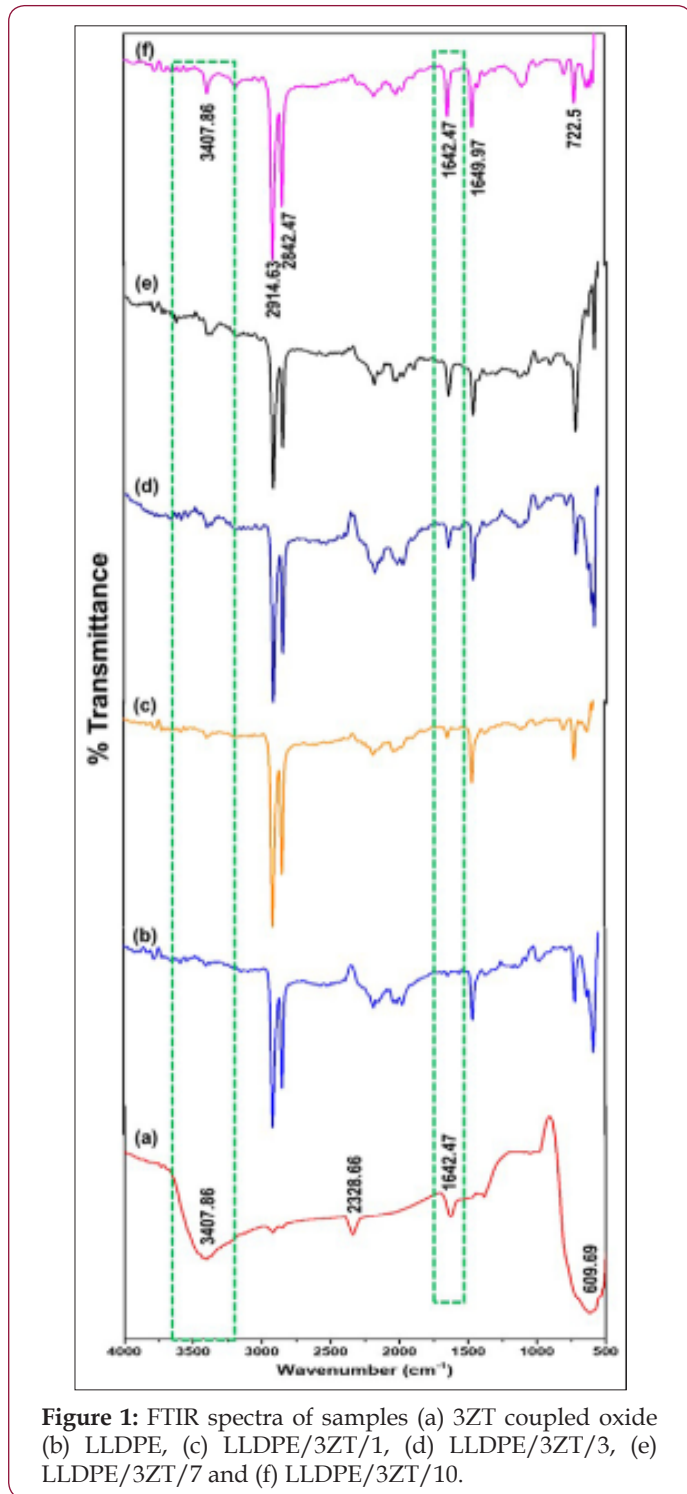
ROS scavenger addition experiments provide information on a variety of reactive candidate that dominate MB photodegradation. This results also provide insights on the reactive candidates that are liable for microbe inactivation. Acetonitrile (ACN), methanol (MeOH) and benzoquinone (BQ) were used as scavengers for hydroxyl radicals, photo-generated holes and superoxide anion radicals, respectively. As seen in Figure 5, a positive correlation was found between MB degradation and wt% of 3ZT coupled oxide. With the addition of the scavengers, the photo-degradation of MB

decelerated drastically with wt% of catalyst, which means more hydroxyl radicals, photogenerated holes and superoxide anion radicals are produced and active during the degradation process.

Upon the introduction of ACN, the photodegradation efficiency of LLDPE with 1wt% to 10wt% 3ZT are decelerated drastically by 32% to 75%, respectively (Table 2).

Table 2: •OH, radical scavenging activity, O₂^{•-} radical scavenging activity and h⁺ scavenging activity of LLDPE nanocomposites.

Sample	OH, radical scavenging activity (%)	O ₂ ^{•-} radical scavenging activity (%)	h ⁺ scavenging activity (%)
LLDPE/3ZT/1	32	12	24
LLDPE/3ZT/3	51	21	41
LLDPE/3ZT/7	75	12	42
LLDPE/3ZT/10	75	15	45



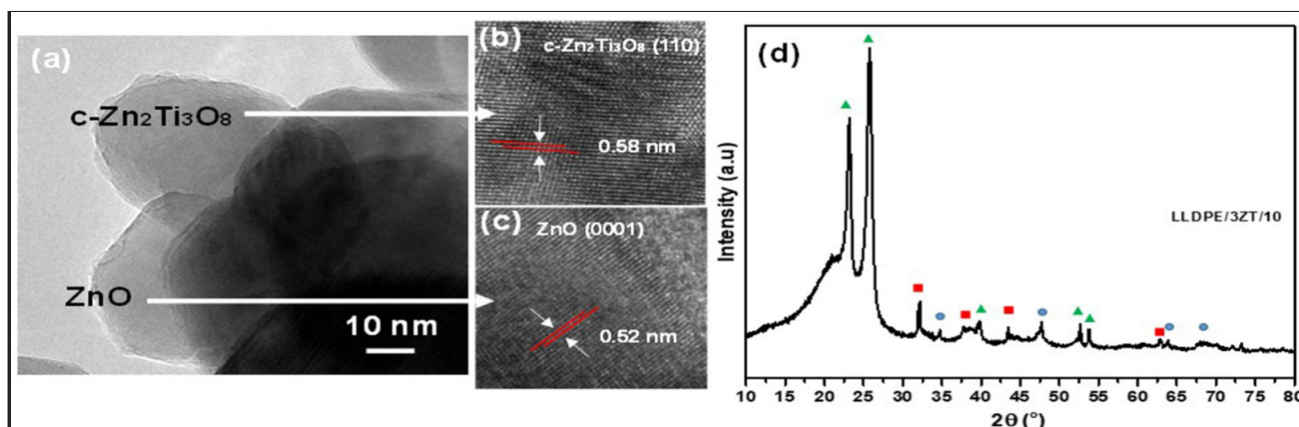


Figure 4: (a) HRTEM image of 3ZT coupled oxides, (c) interplanar spacing of c-Zn₂Ti₃O₈ (d) interplanar spacing of zincite, ZnO structure and (d) XRD pattern of LLDPE/3ZT/10 (LLDPE, zincite, c-Zn₂Ti₃O₈).

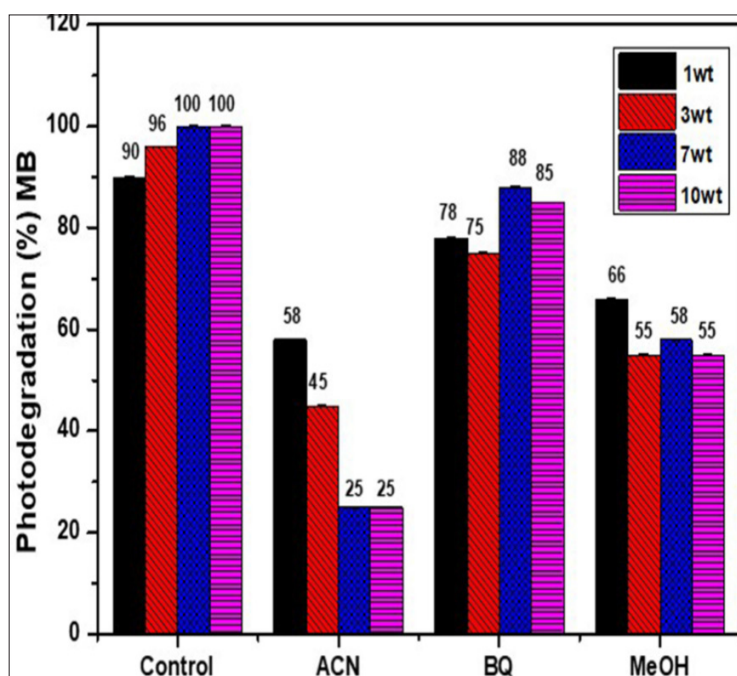


Figure 5: Influence of radical scavengers on the photodegradation of MB over LLDPE/3ZT/1, LLDPE/3ZT/3, LLDPE/3ZT/5, LLDPE/3ZT/7 and LLDPE/3ZT/10, under sunlight: Control (LLDPE Nano-composite with MB alone), BQ as scavenger for O₂⁻ radical, MeOH as scavenger for h⁺, ACN scavenger for [•]OH radical.

The results reveal that [•]OH is the main reactive species of LLDPE Nano-nanocomposites. When BQ is added to the reaction, the photodegradation of MB for LLDPE with 1 to 10wt% changed by 12% to 15%, respectively, indicating minimum contribution of O₂⁻ in LLDPE nanocomposites as compared other reactive candidates towards photodegradation. When MeOH is added, the degradation of all samples is reduced by 24% to 45%, demonstrating another apparent reactive species, h⁺ contribution in photocatalytic reaction. Overall, the photocatalytic results confirm bacteriostatic effect of all LLDPE nanocomposites are primarily driven by three

reactive species in a sequence of [•]OH > h⁺ > O₂⁻. Besides ROS, the interaction of Zn ion released from coupled oxide with bacteria during incubation period will cause cell membrane destructions [33]. Therefore, the Zn ion released from LLDPE composites is analyzed by measuring the dynamic zinc ion by ICP method and displayed in Figure 6. The results show the total concentration of Zn²⁺ release for 12 to 96 h LLDPE nanocomposites immersion at interval of 12h in deionized water. The Zn²⁺ release increases linearly when the weight percentage of 3ZT coupled oxide is increased from 1 – 10 wt.%.

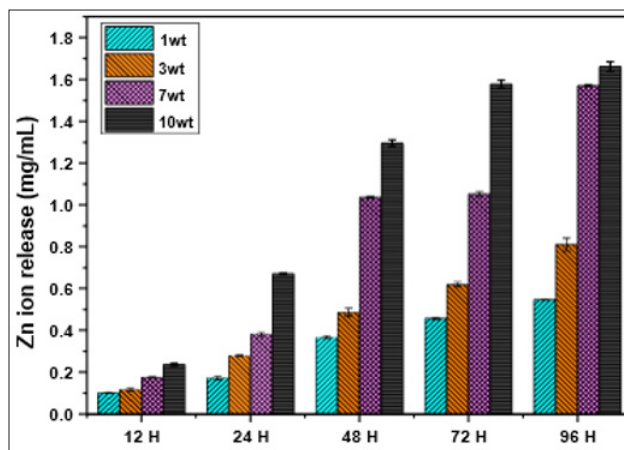


Figure 6: Zn²⁺ release as a function of 3ZT weight percentage.

This behavior is attributed to the ease of water absorption via amorphous region of the LLDPE nanocomposites matrix that has low degree of crystallinity (12-14 %). In this report, LLDPE nanocomposite with 10wt% release a greater amount of Zn²⁺, thus more ions may attach on the teichoic acid on the peptidoglycan layer of Gram positive bacteria and lipopolysaccharides of the Gram-negative bacteria. Attachment of this ion to outer cell wall of bacteria, may cause disruption of the membrane and consequently lead to damage and leakage problems. The antibacterial effect of

LLDPE nanocomposites against *S. aureus* and *E. coli* was verified by bacterial reduction according to ASTM E2149. The percentage bacterial reduction (R%) and numbers of CFU/mL for each sample are presented in Figure 7. According to the standard National Committee for Clinical Laboratory Standards (NCLLS) [34], bactericidal activity is defined when a reduction $\geq 99.9\%$ of the total count of CFU/mL. Whereas, bacteriostatic activity is defined when a reduction between 90% and 99.9% of the total bacteria count (CFU/mL) [35].

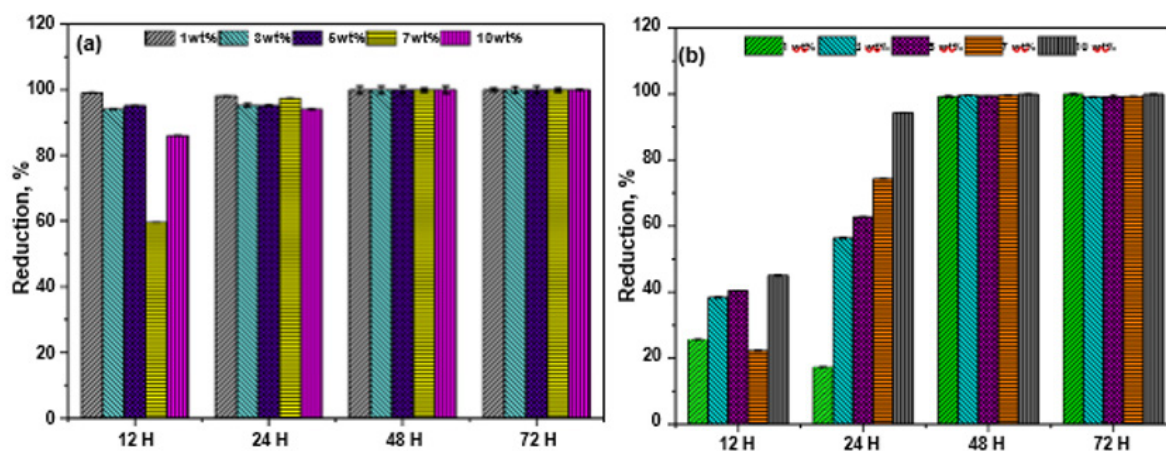


Figure 7: Antibacterial efficiency of LLDPE nanocomposites with different 3ZT weight percent against (a) *S. aureus* and (b) *E. coli*.

Figure 7a shows *S. aureus* cells reduction as a function of time and wt%. As seen, after 12 h, LLDPE nanocomposites inactivate *S. aureus* to some extents. When the incubation time is further extended to 48 h, the inactivation is very high, irrespective of wt% of 3ZT. A 99% reduction of *S. aureus* is attained by LLDPE nanocomposite with 1wt%, presenting enhanced bactericidal effect. This result indicates time of irradiation is an important factor as compare to wt% for high inactivation of *S. aureus*. Nevertheless, the complete 100% inactivation is achieved with LLDPE nanocomposite with 7 and 10wt% 3ZT after 72h of visible light irradiation.

Figure 7b shows represent reduction of *E. coli* cells using a similar set of experiment. As seen, *E. coli* was not susceptible to photocatalytic killing as compared to *S. aureus* for the first 12 h. Nonetheless, when the irradiation time was prolonging to 48 h 99% of *E. coli* was eradicated by all the LLDPE nanocomposites. The bactericidal effect was more pronounced with 100% inactivation when the weight percentage of 3ZT in LLDPE nanocomposite was increased 7 and 10 wt%.

The pronounced bactericidal activity of LDPE nanocomposites with different wt% is affected by several factors such as ROS

release, metal ion release, matrix crystallinity, polarity, and reduced recombination of electron and holes. First of all, the complete inactivation of *S. aureus* and *E. coli* under visible light is achieved in this work because of the heterojunction formation that has significantly improved interfacial structure to facilitate better charge transfer, retain effective charge separation and extend the visible light respond. Besides, the scavenger analysis indicates the bactericidal effect of LLDPE nanocomposites on *S. aureus* and *E. coli* are driven by $\cdot\text{OH}$ radicals and h^+ rather than O_2^- . It has been reported that among ROS, $\cdot\text{OH}$ radicals possess high oxidation potential which attach the bacteria cell more effectively [36] and this might be one of the reasons for pronounced bactericidal activity in the LLDPE nanocomposites incorporated with 3ZT coupled oxides.

The fact that Zn ion concentration is low < 0.2 ppm in the beginning, it indicates *S. aureus* inactivation are dominated by the generation of $\cdot\text{OH}$ radicals and h^+ . The inclusion of oxidative stress through the interaction of $\cdot\text{OH}$ radicals and h^+ with proteins, DNA, and lipids is likely to inactivate the *S. aureus*. There was no

prominent *E. coli* inactivation in LLDPE nanocomposites with low wt% 3ZT for first 12 to 24h. However, as subsequent irradiation time and wt% of 3ZT increased, the Zn ion release were prominent thus accelerate the inactivation of *E. coli*. These results suggest that *E. coli* is found to be more susceptible towards Zn ion. Besides, *E. coli* with a negative surface charge has strong affinity towards the positively charged Zn ion, thus accumulate in cell and disrupt cellular activity and cause cell death.

Apart from that, a superior bacteriostatic effect was found in LLDPE nanocomposite with high percentage of 3ZT (7 and 10wt%) and the reason is due to the relatively low crystallinity and high polarity induced by the hydrophilic characteristic of 3ZT coupled oxides in LLDPE nanocomposite. Such characteristic expedite water uptake through LLDPE matrix, hence promotes high photocatalytic activity to release reactive species as well as Zn ion migration. From the above observation, the mechanism for the *S. aureus* and *E. coli* inactivation of LLDPE nanocomposites with different weight percentage of 3ZT is illustrated in Figure 8.

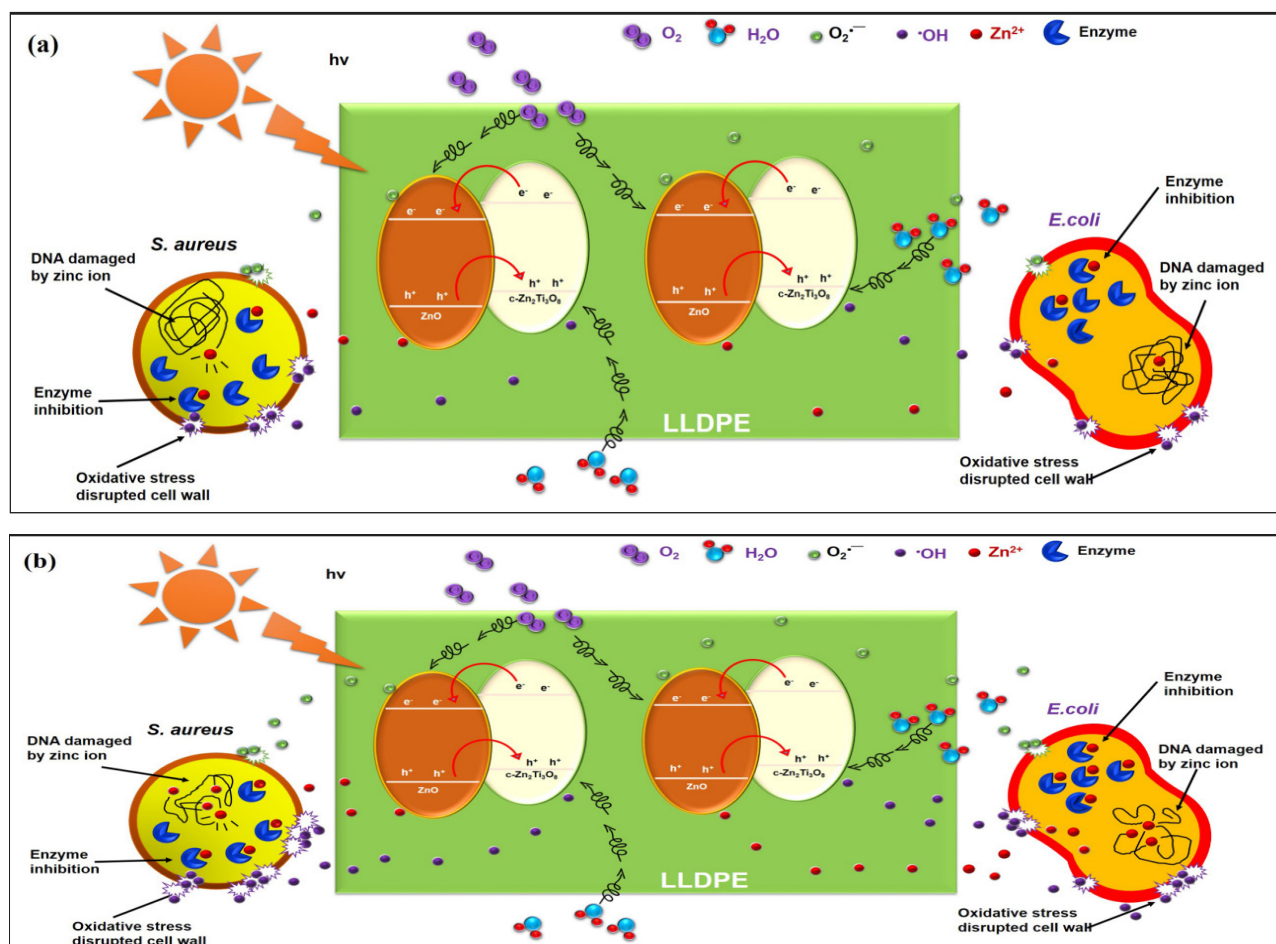


Figure 8: Antimicrobial mechanism of LLDPE/3ZT nanocomposites against *S. aureus* and *E. coli*. ROS generation, DNA binding and enzyme inhibition by Zn^{2+} taking place at the cellular level leading to cell death. (a) shows low amount of ROS and Zn^{2+} production by LLDPE ≤ 7 wt% 3ZT, (b) shows massive production of ROS and Zn^{2+} by LLDPE ≥ 7 wt% 3ZT, leading to fast killing.

Conclusion

From the above observation, it is found that the incorporation of 3ZT into LLDPE exhibit good inactivation of *S. aureus* and *E. coli* under visible light. With increasing weight percent of 3ZT, the $\cdot\text{OH}$ radical formed increased and enhance the photocatalytic inactivation of *S. aureus*. The pronounce *E. coli* inactivation characteristic with high weight percent of 3ZT and longer incubation time show Zn^{2+} play a major role for inactivation of *E. coli*. Other factor such as low degree of crystallinity, high charge carrier separation induced by hetero-junction formation also play an important role to inactivation of *S. aureus* and *E. coli*.

Acknowledgement

The authors are thankful to the Ministry of Education (MOE) Malaysia for funding this work under Transdisciplinary Research Grant Scheme (TRGS) grant no. 6769002. The authors are very much grateful to Universiti Sains Malaysia (USM) for providing the necessary facilities to carry out the research work.

References

- W Blackburn C, McClure PJ (2009) Foodborne pathogens: hazards, risk analysis and control. Elsevier.
- Guan Y, Xiao H, Sullivan H, Zheng A (2007) Antimicrobial-modified sulfite pulps prepared by in situ copolymerization. Carbohydrate polymers 69: 688-696.
- Thome J, Holländer A, Jaeger W, Trick I, Oehr C (2003) Ultrathin antibacterial polyammonium coatings on polymer surfaces. Surface and Coatings Technology 174: 584-587.
- Perez-Perez C, Regalado-González C, Rodríguez-Rodríguez C, Barbosa-Rodríguez J (2006) Villaseñor-Ortega F. Incorporation of antimicrobial agents in food packaging films and coatings. Advances in agricultural and food biotechnology 37: 2.
- Zhang H, Hortal M, Jordá-Beneyto M, Rosa E, Lara-Lledo M, Lorente I (2017) ZnO-PLA nanocomposite coated paper for antimicrobial packaging application. LWT-Food Science and Technology 78: 250-257.
- Palza H, Quijada R, Delgado K (2015) Antimicrobial polymer composites with copper micro- and nanoparticles: Effect of particle size and polymer matrix. Journal of Bioactive and Compatible Polymers 30: 366-380.
- Emamifar A, Mohammadzadeh M (2015) Preparation and application of LDPE/ZnO nanocomposites for extending shelf life of fresh strawberries. Food technology and biotechnology 53: 488.
- Jašková V, Hochmannová L, Vytřasová J (2013) TiO_2 and ZnO nanoparticles in photocatalytic and hygienic coatings. International journal of photoenergy.
- Khan ST, Al-Khedhairi AA, Musarrat J (2015) ZnO and TiO_2 nanoparticles as novel antimicrobial agents for oral hygiene: a review. Journal of Nanoparticle Research 17: 276.
- Yañez D, Guerrero S, Lieberwirth I, Ulloa MT, Gomez T (2015) Photocatalytic inhibition of bacteria by TiO_2 nanotubes-doped polyethylene composites. Applied Catalysis A General 489: 255-261.
- Prasanna K, Sailaja R (2012) Blends of LDPE/chitosan using epoxy-functionalized LDPE as compatibilizer. Journal of Applied Polymer Science 124: 3264-3275.
- Llorens A, Lloret E, Picouet PA, Trbojevič R, Fernandez A (2012) Metallic-based micro and nanocomposites in food contact materials and active food packaging. Trends in Food Science & Technology 24: 19-29.
- Chawengkijwanich C, Hayata Y (2008) Development of TiO_2 powder-coated food packaging film and its ability to inactivate *Escherichia coli* in vitro and in actual tests. International journal of food microbiology 123: 288-292.
- Zan L, Fa W, Peng T, Gong Zk (2007) Photocatalysis effect of nanometer TiO_2 and TiO_2 -coated ceramic plate on Hepatitis B virus. Journal of Photochemistry and Photobiology B: Biology 86: 165-169.
- Hajkova P, Spatenka P, Horsky J, Horska I, Kolouch A (2007) Photocatalytic effect of TiO_2 films on viruses and bacteria. Plasma Processes and Polymers pp. 4.
- Ramesh T, Nayak B, Amirbahman A, Tripp CP, Mukhopadhyay S (2016) Application of ultraviolet light assisted titanium dioxide photocatalysis for food safety: A review. Innovative Food Science & Emerging Technologies 38: 105-115.
- (2015) Color Additives Approved for Use in Drugs, Part 73, Subpart B: Color Additives Exempt from Batch Certification (Zinc Oxide) U.S. Food and Drug Administration, Food and Drugs: Silver Spring, MD, USA.
- Sakthivel S, Neppolian B, Shankar M, Arabindoo B, Palanichamy M, Murugesan V (2003) Solar photocatalytic degradation of azo dye: comparison of photocatalytic efficiency of ZnO and TiO_2 . Solar Energy Materials and Solar Cells 77: 65-82.
- Wang Y, Ma J, Xu Q, Zhang J (2017) Fabrication of antibacterial casein-based ZnO nanocomposite for flexible coatings. Materials & Design 113: 240-245.
- Azam A, Ahmed AS, Oves M, Khan MS, Habib SS, Memic A (2012) Antimicrobial activity of metal oxide nanoparticles against Gram-positive and Gram-negative bacteria: a comparative study. International journal of nanomedicine 7: 6003.
- Sangshetti JN, Dharmadhikari PP, Chouthe RS, Fatema B, Lad V, (2013) Microwave assisted nano (ZnO- TiO_2) catalyzed synthesis of some new 4, 5, 6, 7-tetrahydro- 6-((5-substituted-1, 3, 4-oxadiazol-2-yl) methyl) thieno [2, 3-c] pyridine as antimicrobial agents. Bioorganic & medicinal chemistry letters 23: 2250-2253.
- Khan ST, Al-Khedhairi AA, Musarrat J (2015) ZnO and TiO_2 nanoparticles as novel antimicrobial agents for oral hygiene: a review. Journal of Nanoparticle Research 17: 276.
- Meftahi A, Yadegari F, Alibakhshi S, Vatandoost S, Mohammadi H (2015) Finishing of Nylon/Cotton Fabric with ZnO/ TiO_2 Nanocomposite. Procedia Materials Science 11: 600-604.
- Saharudin KA, Sreekantan S, Basiron N, Khor YL, Harun NH (2018) Bacteriostatic Activity of LLDPE Nanocomposite Embedded with Sol-Gel Synthesized TiO_2 /ZnO Coupled Oxides at Various Ratios. Polymer 10: 878-895.
- Fahim IS, Mamdouh W, Salem H (2015) Effect of Processing Technique on LDPE Thin Films and sheets.
- Ali SS, Qazi IA, Arshad M, Khan Z, Voice TC, Mehmood CT (2016) Photocatalytic degradation of low density polyethylene (LDPE) films using titania nanotubes. Environmental Nanotechnology, Monitoring & Management 5: 44-53.
- Fuad M, Hanim H, Zarina R, Ishak Z, Hassan A (2010) Polypropylene/calcium carbonate nanocomposites--effects of processing techniques and maleated polypropylene compatibiliser. Express Polymer Letters p. 4.
- Al Rawajfeh AE, Al Salahb HA, Al Rhaelc I (2006) Miscibility, Crystallinity and Morphology of Polymer Blends of Polyamide-6/Poly (β -hydroxybutyrate).
- Al Johani MS, Al Zaghayer Y, Al Mayman SI (2015) TiO_2 /ZnO photocatalytic activity for hydrogen production. Int Sci J Environ Sci 4: 1-8.
- Rajbongshi BM, Samdarshi S, Boro B (2015) Multiphasic bi-component TiO_2 -ZnO nanocomposite: synthesis, characterization and investigation

of photocatalytic activity under different wavelengths of light irradiation. Journal of Materials Science: Materials in Electronics 26: 377-384.

31. Kuila T, Bose S, Mishra AK, Khanra P, Kim NH, Lee JH (2012) Effect of functionalized graphene on the physical properties of linear low-density polyethylene nanocomposites. Polymer Testing 31: 31-8.
32. Kong H, Song J, Jang J (2010) Photocatalytic antibacterial capabilities of TiO₂- biocidal polymer nanocomposites synthesized by a surface-initiated photopolymerization. Environmental science & technology 44: 5672-5676.
33. Pasquet J, Chevalier Y, Pelletier J, Couval E, Bouvier D, Bolzinger MA (2014) The contribution of zinc ions to the antimicrobial activity of zinc oxide. Colloids and Surfaces A: Physicochemical and Engineering Aspects 457: 263-274.
34. Barry AL, Craig WA, Nadler H, Reller LB, Sanders CC, Swenson JM. Methods for determining bactericidal activity of antimicrobial agents: approved guideline. NCCLS document M26-A 1999: 19.
35. Pankey G, Sabath L (2004) Clinical relevance of bacteriostatic versus bactericidal mechanisms of action in the treatment of Gram-positive bacterial infections. Clinical infectious diseases 38: 864-870.
36. Birben E, Sahiner UM, Sackesen C, Erzurum S, Kalayci O (2012) Oxidative stress and antioxidant defense. World Allergy Organization Journal 5: 9.

ISSN: 2574-1241

DOI: [10.26717/BJSTR.2018.08.001681](https://doi.org/10.26717/BJSTR.2018.08.001681)

Srimala Sreekantan. Biomed J Sci & Tech Res



This work is licensed under Creative Commons Attribution 4.0 License

Submission Link: <https://biomedres.us/submit-manuscript.php>



Assets of Publishing with us

- Global archiving of articles
- Immediate, unrestricted online access
- Rigorous Peer Review Process
- Authors Retain Copyrights
- Unique DOI for all articles

<https://biomedres.us/>